Decomposition of Hydrogen Peroxide at Water−Ceramic Oxide Interfaces

A. Hiroki and Jay A. LaVerne*

Radiation Laboratory, University of Notre Dame, Notre Dame, Indiana 46556

Received: August 10, 2004; In Final Form: December 6, 2004

The thermal decomposition of hydrogen peroxide, H_2O_2, was determined in aqueous suspensions of SiO_2, Al_2O_3, TiO_2, CeO_2, and ZrO_2 nanometer-sized particles. First-order kinetics were observed for the decomposition in all cases. Temperature dependence studies found that the activation energy was 42 ± 5 kJ/mol for the overall decomposition of H_2O_2 independent of the type of oxide. Oxide type had a strong effect on the preexponential rate term with increasing rate in the order of $SiO_2 < Al_2O_3 < TiO_2 < CeO_2 < ZrO_2$. The rate coefficient for H_2O_2 decomposition increases with increasing surface area of the oxide, but the number or efficiency of reactive sites rather than the total surface area may have the dominant role. Very efficient scavengers for OH radicals in the bulk liquid are not able to prevent formation of molecular oxygen, the main H_2O_2 gaseous decay product, suggesting that decomposition occurs on the oxide surfaces. The decomposition of H_2O_2 in the γ-radiolysis of water is enhanced by the addition of ceramic oxides, possibly due to excess formation of hydrated electrons from energy deposited in the solid.

Introduction

The strong oxidants produced in the decomposition of hydrogen peroxide, H_2O_2, have been examined in a number of contexts including supercritical fluid oxidation, environmental remediation, and nuclear reactor corrosion.[1−3] The proposed mechanisms vary widely, but a commonality in many instances seems to be decomposition in association with a solid interface. Chain reactions of hydrogen peroxide with some metals can be readily explained by invoking the well-known Haber−Weiss mechanism.[4] However, the decomposition of hydrogen peroxide in the presence of many ceramic oxides does not occur in this manner because of the lack of available oxidation states of the cation or because a chain process is not involved. The fundamental aspects of the decomposition of aqueous solutions of hydrogen peroxide at the surface of ceramic oxides are not well-characterized, yet this process may have implications in a wide variety of important environmental and energy production applications.

Pyrolysis of H_2O_2 vapor has been the subject of a few earlier investigations.[5−8] At high temperature (>400 °C), the decomposition is thought to be initiated by O−O bond cleavage to give two OH radicals, followed by two simple reactions.

$$H_2O_2 \rightarrow 2OH \qquad \text{(R1)}$$

$$OH + H_2O_2 \rightarrow HO_2 + H_2O \qquad \text{(R2)}$$

$$2HO_2 \rightarrow H_2O_2 + O_2 \qquad \text{(R3)}$$

The stoichiometric relationship gives half of an oxygen molecule for every H_2O_2 molecule decomposed.

$$H_2O_2 \rightarrow H_2O + {}^1/_2O_2 \qquad \text{(R4)}$$

Activation energies of 180 and 200 kJ/mol were determined in good agreement with an O−O bond dissociation energy of about 210 kJ/mol.[5,6,9] More recent studies on the thermal decomposition of H_2O_2 in liquid water[10] and supercritical water[1] have found different overall rates with activation energies of 71 and 180 kJ/mol, respectively. The initial H_2O_2 decomposition step in the liquid or supercritical phase is generally assumed to be

$$H_2O_2 + M \rightarrow 2OH + M \qquad \text{(R1a)}$$

where M is a water molecule. Dissociation of all species must be considered in the liquid phase since the pK_a values of H_2O_2, HO_2, and OH are 11.8, 4.88, and 11.9, respectively.[10] In neutral water, only the HO_2 dissociation needs to be considered

$$HO_2 \leftrightarrow H^+ + O_2^- \qquad \text{(R5)}$$

and the following equation is often included in the scheme with reactions R2 and R3.

$$OH + HO_2(O_2^-) \rightarrow O_2 + H_2O(OH^-) \qquad \text{(R6)}$$

The overall stoichiometry is still given by reaction R4.

The decomposition of H_2O_2 in the presence of various solid oxide particles also has been investigated.[11−28] Several different methods have been proposed for the decomposition of H_2O_2 in these systems. A wide variety of reaction pathways is possible because of the differences in the properties of the oxides. For example, the oxidation of ferrous oxide by H_2O_2 occurs with the formation of the ferric cation, which is also highly reactive toward H_2O_2, leading to a chain process.[26] However, no higher oxidation states exist for the cations in oxides such as CeO_2 or ZrO_2. Other mechanisms for H_2O_2 decomposition must occur in these systems, and the mechanism may involve simple O−O bond cleavage as in pyrolysis, oxidation of an oxygen site, or some other process that presumably occurs at the surface. The overall decomposition of H_2O_2 is expected to follow reaction R1a with M as a yet undefined site but presumably on the oxide surface.

The photolysis of aqueous H_2O_2 solutions is initiated by the direct cleavage of the O−O bond, which should be relatively

* Author to whom correspondence should be addressed. Phone: (574) 631-5563. Fax: (574) 631-8068. E-mail: laverne.1@nd.edu.

10.1021/jp046405d CCC: $30.25
Published on Web 01/22/2005

independent of the local environment unless the molecule is adsorbed on a surface.[29,30] Recently, it has been reported that various organic contaminants in water can be oxidized effectively by the OH radical produced by the photolysis of H_2O_2 in the presence of metal oxides.[31−36] Destruction of harmful organic compounds by these oxidation techniques is gaining widespread attention as an advanced oxidation technology. The decomposition of H_2O_2 in the radiolysis of aqueous solutions is initiated by water decomposition products, i.e., hydrated electrons, H atoms, and OH radicals, which can lead to very different results than those in photolysis.[37−42] Furthermore, radiolytic products are known to be affected by the presence of ceramic oxides.[43] Radiolytic systems involving aqueous H_2O_2 solutions in proximity to solid oxide interfaces can be extremely complicated. Corrosion in the core and the circulation lines of pressurized boiling water reactors due to the oxidizing species produced in the radiolytic decomposition of H_2O_2 is a major problem of vital importance to energy production.[44−46]

In this work, the decomposition of aqueous H_2O_2 solutions was examined as a function of temperature in the presence of SiO_2, Al_2O_3, TiO_2, CeO_2, and ZrO_2 nanometer-sized particles. Effects of surface area on the rate of H_2O_2 decomposition were determined. Gaseous products were analyzed with and without selected radical scavengers to probe potential reaction pathways. The radiolytic decomposition of H_2O_2 in aqueous solutions was examined as a function of added ceramic oxides, and the results were discussed with respect to thermal decomposition.

Experimental Section

The solutions used in this study were prepared using water from a Millipore Milli-Q UV system. Aqueous solutions of initial 5 μM to 50 mM H_2O_2 were prepared from 30% hydrogen peroxide standard solution (Fisher Scientific). Suspensions for examining thermal decomposition were made with 3 mL of H_2O_2 solution and 0.1−0.5 g of oxide while those for gas production were 2 mL of H_2O_2 solution and 0.25 g of oxide. The oxides were silica (SiO_2, Alfa Aesar), alumina (Al_2O_3, Alfa Aesar), titania (TiO_2, Aldrich), ceria (CeO_2, REacton from Alfa Aesar), or zirconia (ZrO_2, Alfa Aesar). Particle surface areas were determined on a Quantachrome Autosorb 1 analyzer using nitrogen adsorption and desorption at equilibrium vapor pressure and the Brunauer−Emmet−Teller (BET) method of surface area calculation. Specific surface areas of SiO_2, Al_2O_3, TiO_2, CeO_2, and ZrO_2 particles were determined to be 7.91, 8.09, 2.52, 7.21, and 1.59 m^2/g, respectively. The densities of the oxides are 2.2, 3.97, 3.9, 7.13, and 5.89 g/cm^3, respectively. Perfect spheres have a specific surface area equal to $6/\rho d$, where ρ is the density and d is the diameter. The estimated particle diameters are 345, 187, 611, 117, and 641 nm for SiO_2, Al_2O_3, TiO_2, CeO_2, and ZrO_2, respectively.

All sample cells were made from 10 mm diameter Pyrex tubes into which the aqueous mixtures were added, sealed with rubber septa, purged with ultrahigh purity helium or argon, and permanently heat-sealed. Final cell length was about 10 cm, and the cell was approximately half-filled with the aqueous mixture. Experiments for the decomposition of H_2O_2 at elevated temperature (25−120 °C) were performed using an oven specifically designed to snugly hold the sample cell for rapid heating.[42] During the decomposition, the heater was shaken to provide complete mixing of the suspension. The sample cells were removed from the heater at various time intervals, then immediately immersed in ice−water to suppress further thermal decomposition of the H_2O_2. The sample solutions were then filtered through a Millipore filter (pore size, 0.25 μm) to separate the oxide from the solution.

Irradiations were carried out using a Gammacell-220 ^{60}Co source in the Radiation Laboratory at the University of Notre Dame. The dose rate was 9.8 Gy/min (0.98 krad/min) as determined using the Fricke dosimeter.[41,47] The total absorbed dose was varied up to 590 Gy at room temperature. Irradiations were performed with initial H_2O_2 concentrations of 50 and 500 μM. Complete mixing of the aqueous mixture throughout the irradiation was ensured by using a Teflon chip coupled to a magnetic stirrer. After the irradiation, the sample was filtered as described above and analyzed for H_2O_2.

The concentration of hydrogen peroxide was determined by the Ghormley triiodide method in which I^- is oxidized to I_3^- by the H_2O_2.[48,49] Absorbances were measured at 350 nm (the wavelength of maximum absorption for I_3^-), using a diode array spectrophotometer (Hewlett-Packard HP8453). The molar extinction coefficient of I_3^- at 350 nm was taken as 25500 M^{-1} cm^{-1}.[42] Error limits for the H_2O_2 concentrations are estimated to be about 5%.

Gaseous oxygen and hydrogen were determined using a SRI 8610 gas chromatograph following a technique as previously reported.[43] Argon was used as the carrier gas for hydrogen and helium for oxygen. After the irradiation, the sample cells were placed in a section of Tygon tubing isolated from the gas chromatograph carrier gas with a four-way valve. The section was purged, the cell was crushed, and the gases were injected into the carrier gas stream. Calibration of the gas chromatograph was performed by injecting pure gases with a gastight microliter syringe. Error in gas measurement is estimated to be about 5%.

Results and Discussion

Thermal Decomposition Kinetics of H_2O_2. Virtually all of the previous studies on the thermal and catalytic decomposition of H_2O_2 report first-order decay kinetics, and similar results are expected in the present work.[1,5,9,25] For a first-order decay as described by reaction R1, the observed loss of H_2O_2 can be written as

$$\frac{-\mathrm{d}[H_2O_2]}{\mathrm{d}t} = k_{obs}t \quad \text{or} \quad \ln\left(\frac{[H_2O_2]}{[H_2O_2]_0}\right) = -k_{obs}\mathrm{t} \qquad (1)$$

where k_{obs} is the observed decomposition rate coefficient, t is the resident time at temperature, and $[H_2O_2]_0$ and $[H_2O_2]$ are the H_2O_2 concentrations before and after heating, respectively. In an aqueous solution or in the presence of a catalysis, the decomposition of H_2O_2 is formally a second-order process given by reaction R1a, but the concentration of M can be assumed to be invariant giving a pseudo-first-order rate of decay. Equation 1 offers a simple method for extracting the observed rate coefficient and was used to analyze the thermal decays. Comparison of the temperature dependences of the rate coefficients for the various oxides should give information on the commonality of the mechanisms involved.

Aqueous solutions of H_2O_2 were quickly brought to temperature for a fixed period of time, then rapidly cooled, filtered, and analyzed. Concentrations of H_2O_2 were determined as close as possible immediately before and after resident heating times. Typical results for $\ln([H_2O_2]/[H_2O_2]_0)$ are shown in Figure 1 as a function of the resident time at temperature. This particular set of data is for 5 μM H_2O_2 in the presence of 0.1 g (~3 wt %) Al_2O_3 at 80, 100, and 120 °C. A linear dependence is observed at each temperature, indicating that the decomposition of H_2O_2 in the presence of Al_2O_3 follows first-order kinetics. The rate coefficients extracted from the slopes of the lines fitted to the data of Figure 1 give rate coefficients of 7.9×10^{-5}, 2.0

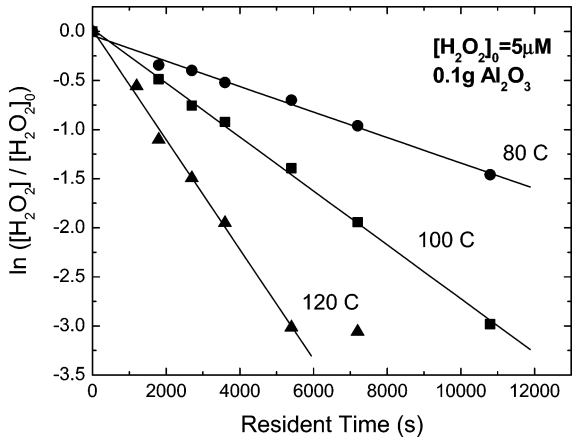

Figure 1. The relative loss of 5 μM H_2O_2 with 0.1 g of Al_2O_3 as a function of resident time at 80 (●), 100 (■), and 120 °C (▲).

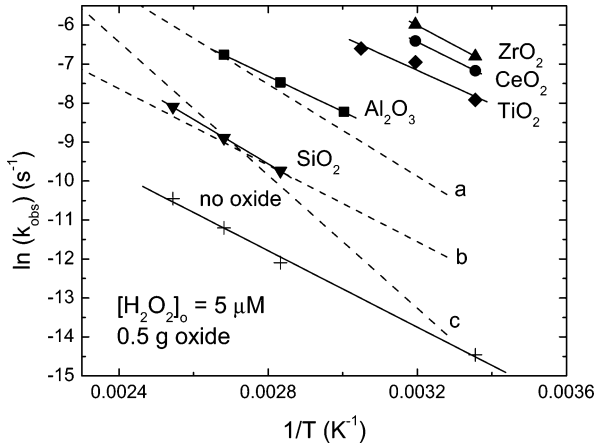

Figure 2. Arrhenius plots of ln(k_{obs}) as a function of inverse temperature for no added oxide (+), SiO_2 (▼), Al_2O_3 (■), TiO_2 (◆), CeO_2 (●), and ZrO_2 (▲). The suspensions were 0.5 g of oxide in 3 mL of solution, 14 wt %. Dashed line a is for the homogeneous rate, and dashed line b is for the wall or heterogeneous rate in subcritical liquid water, ref 1. Dashed line c is for liquid water, ref 9.

$\times 10^{-4}$, and 4.8×10^{-4} s^{-1} at 80, 100, and 120 °C, respectively. A lower limit to ln([H_2O_2]/[H_2O_2]$_0$) of about −3 is due to the lower detection limit of the analytical technique. Similar first-order dependencies were observed for the decay of H_2O_2 in the presence of SiO_2, TiO_2, CeO_2, and ZrO_2 and in the absence of any added oxide.

The half-life (0.693/k_{obs}) for the decay of H_2O_2 in the presence of 0.1 g Al_2O_3 at 80 °C is 146 min and decreases to about 24 min at 120 °C. A temperature-dependent decay rate can be analyzed by the standard Arrhenius equation

$$k_{obs} = A\, e^{-E_a/RT} \quad \text{or} \quad \ln(k_{obs}) = \ln(A) - \frac{E_a}{RT} \qquad (2)$$

where E_a is the activation energy, A is the frequency factor, R is the gas constant (8.314 J/(mol K)), and T is the absolute temperature. Arrhenius plots for the decomposition of H_2O_2 in the presence of 0.5 g (∼14 wt %) each of SiO_2, Al_2O_3, TiO_2, CeO_2, or ZrO_2 and in the absence of any added oxide are shown in Figure 2. The lines shown in Figure 2 are least-squares fit to the data. Good straight line fits indicate that the rate coefficients follow the Arrhenius form. The rate of H_2O_2 decomposition is slowest in the absence of oxide, which is really about 3×10^{-3} m^2 of Pyrex (SiO_2) compared to the 1−4 m^2 for 0.5 g of the other oxides. This set of data may also be influenced by any residual impurities from H_2O_2 synthesis. Impurities should not affect the results with added oxides because of the very large surface areas involved. Oxide addition obviously increases the rate of H_2O_2 decomposition. The decomposition rate increases in the order of SiO_2 < Al_2O_3 < TiO_2 < CeO_2 < ZrO_2. Certain experimental limitations precluded extending the data over a wider temperature range. At very low decomposition rates, the change in H_2O_2 concentration was impractical to measure except for the Pyrex cell without oxide. The highest working temperature was 120 °C where the vapor pressure is already greater than 2 atm and rupture of the Pyrex cell is likely. The decay of H_2O_2 with CeO_2 and ZrO_2 is so fast above 40 °C that significant uncertainties arose in determining accurate resident temperature times.

TABLE 1: Arrhenius Parameters and Half-Lives of H_2O_2 Decay in Aqueous Mixtures of 0.5 g of Different Oxides

	activation energy E_a (kJ mol^{-1})	frequency factor A (s^{-1})	$\tau_{1/2}$ 25 °C (s)	$\tau_{1/2}$ 100 °C (s)
no oxide (Pyrex)	41	6.9×10^0	1.5×10^6	5.5×10^4
SiO_2 (0.5 g)	48	6.2×10^2	2.9×10^5	4.3×10^3
Al_2O_3 (0.5 g)	38	2.3×10^2	1.4×10^4	6.3×10^2
TiO_2 (0.5 g)	36	8.0×10^2	1.8×10^3	1.4×10^2
CeO_2 (0.5 g)	40	6.5×10^3	1.1×10^3	4.3×10^1
ZrO_2 (0.5 g)	42	3.0×10^4	5.3×10^2	1.7×10^1

Equation 2 shows that the activation energy for H_2O_2 decomposition is proportional to the slope of the lines through the data of Figure 2. It is readily observable from the data in Figure 2 that similar activation energies are expected for all the oxides examined here. Values for the activation energy and the frequency factor for H_2O_2 decomposition with 0.5 g of the different oxides are summarized in Table 1. Although the frequency factor varied with oxide type, common activation energies of about 42 ± 0.5 kJ/mol are found. Previous work by Croiset et al. examined the decomposition of H_2O_2 in aqueous solutions and found a very strong dependence of the observed or global rate coefficient on the surface-to-volume ratio of added Inconel.[1] By varying the surface-to-volume ratio, they were able to extract homogeneous and heterogeneous (wall-affected) rate coefficients with activation energies of 49 and 40.8 kJ/mol, respectively, for liquid water at subcritical temperatures. The predicted rates from this work are given in Figure 2 as the dashed lines a and b, respectively, and agree well with the present results. Takagi and Ishigure were able to determine the H_2O_2 decomposition rates using complete mixing or plug flow type reactors, the latter being more affected by the reactor walls.[9] They determine activation energies of 71 and 54 kJ/mol, respectively. They only give an absolute rate for the complete mixing case, which is shown as the dashed line c in Figure 2. The agreement of the different sets of data is good considering the uncertainties involved. A common activation energy in all cases suggests that the rate-determining step for the decomposition of H_2O_2 is similar, if not the same, in the presence of these oxides. Furthermore, the observed activation energy of about 40 kJ/mol is considerably less than the 210 kJ/mol for the cleavage of the O−O bond in H_2O_2, so the water−oxide interface is lowering the energy barrier for H_2O_2 decomposition.

Effects of Oxide Surface Area on H_2O_2 Decomposition Rate. The common activation energy found for all of the oxides examined here suggests that the H_2O_2 decomposes by the same mechanism for each. The reactions occurring on a surface usually include several steps such as diffusion of the reacting molecules to the surface, adsorption on the surface (the reactive sites), reaction on the surface, desorption of products, and diffusion of the desorbed products. One of these steps is

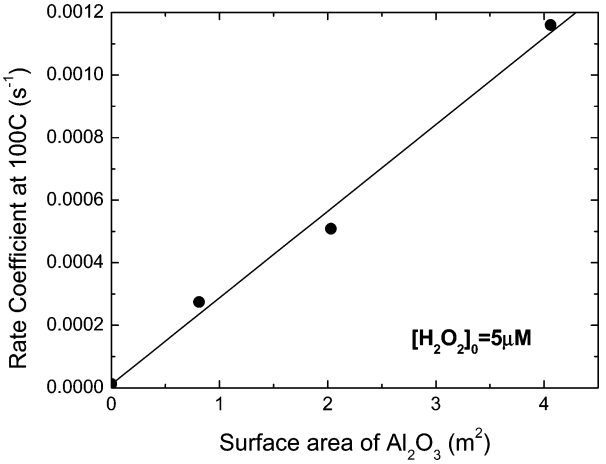

Figure 3. Rate coefficients for the decomposition of H_2O_2 at 100 °C as a function of the Al_2O_3 surface area.

TABLE 2: Oxide Properties and Surface Area normalized Arrhenius Parameters for H_2O_2 Decay in Aqueous Mixtures of Different Oxides

	specific surface area (m^2/g)	density (g/cm^3)	particle diameter (nm)	band gap energy (eV)	pseudo-frequency factor A (s^{-1} m^{-2})
SiO_2	7.91	2.2	345	11.0	1.3×10^2
Al_2O_3	8.09	3.97	187	9.5	1.6×10^2
TiO_2	2.52	3.9	611	3.0	6.4×10^2
CeO_2	7.21	7.13	117	3.0	1.7×10^3
ZrO_2	1.59	5.89	641	5.0	3.8×10^4

expected to be limiting the rate of H_2O_2 decomposition for the oxides examined here.

The data shown in Figure 2 were all performed at 0.5 g of oxide to show comparison between the different oxides. However, each oxide is a different sized particle, with a corresponding variation in surface area. One would like to determine if just the presence of additional surface area is leading to the observed variation in H_2O_2 decomposition. Particle sizes as determined from the measured surface areas are given in Table 2. To further examine the effect of surface area, the decomposition rates were more thoroughly examined using Al_2O_3. The rate of H_2O_2 decomposition in the presence of 0.1 g of Al_2O_3, as in Figure 1, was slower than that in the presence of 0.5 g of Al_2O_3. The temperature dependence for H_2O_2 decomposition, not shown, gives the same activation energy at 0.1 and 0.5 g of Al_2O_3 with differences only in the frequency factors. The effect of the surface area on H_2O_2 decomposition was explored in aqueous solutions with Al_2O_3 at 100 °C. An initial H_2O_2 concentration of 5 μM was used in the experiments. A linear decrease of $\ln([H_2O_2]/[H_2O_2]_0)$ as a function of resident time at temperature was observed for all aqueous solutions of H_2O_2 with 0−0.5 g of Al_2O_3. The variation of the observed rate coefficients for H_2O_2 decomposition calculated from the slopes of the straight line decays are shown as a function of surface area of Al_2O_3 in Figure 3. It can be seen that the rate coefficient of H_2O_2 decomposition at 100 °C is directly proportional to the surface area of Al_2O_3.

A comparison between the decay rates for the different oxides normalized to the particle surface area will show if H_2O_2 decomposition is due just to the presence of an interface or if specific sites are involved. Assuming a linear relationship between the rate coefficient and oxide surface area, as suggested in Figure 3, the observed rate coefficients for H_2O_2 decomposition, k_{obs}, were modified to give $k' = k_{obs}/SW$, where k' is a pseudo-first-order rate coefficient (s^{-1} m^{-2}) with respect to the surface area, S is the specific surface area of the oxide (m^2/g), and W is the weight of the oxide (g). The rate coefficients for H_2O_2 decomposition in the presence of the oxides were recalculated on this basis and shown in Figure 4. The surface-normalized frequency factors are listed in Table 2. Since k' represents the rate coefficient of H_2O_2 decomposition per unit of surface area, it can be seen from Figure 4 that the rate-determining step for H_2O_2 decomposition is not the total surface area. The results suggest that selective reactive sites are responsible for H_2O_2 decomposition, and their number per unit of surface area varies with oxide type. Alternatively, if each oxide is subsequently determined to have similar numbers of sites per unit of surface, then the efficiencies of these sites must be different. Scaling of the data of Figure 4 shows that the relative number or efficiency of reactive sites per unit of surface area varies by 1:1.2:4.9:12.6:289 for SiO_2, Al_2O_3, TiO_2, CeO_2, and ZrO_2, respectively.

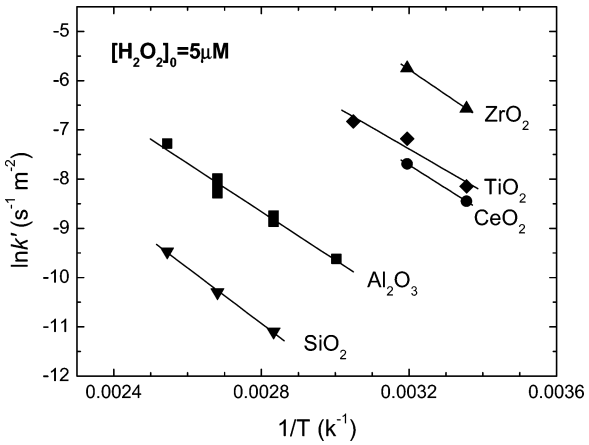

Figure 4. Arrhenius plots of the surface-area-normalized pseudo-first-order decay-rate coefficient $\ln(k' = k_{obs}/\text{surface area})$ as a function of inverse temperature for SiO_2 (▼), Al_2O_3 (■), TiO_2 (◆), CeO_2 (●), and ZrO_2 (▲).

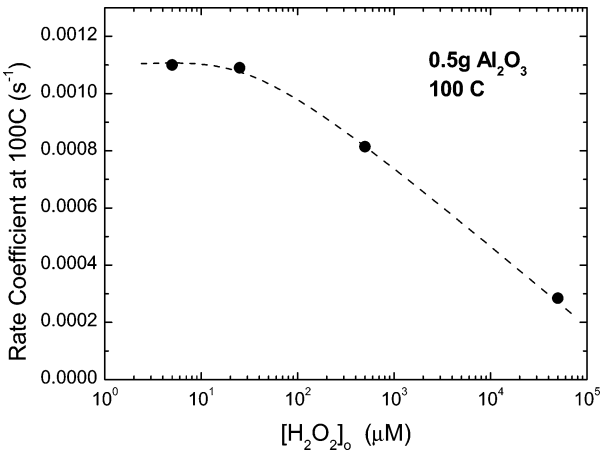

Figure 5. Rate coefficients for the decomposition of H_2O_2 as a function of its initial concentration in aqueous solution of 0.5 g (14 wt %) of Al_2O_3.

Effects of Initial H_2O_2 Concentration on Its Decomposition. Experiments were carried out in the presence of 0.5 g of Al_2O_3 to determine the effects of initial H_2O_2 concentration on the decomposition rate. The observed first-order decays suggest that the H_2O_2 decomposition rate is independent of its initial concentration. To further examine this property, the initial concentration of H_2O_2 was varied between 5 μM and 50mM. Figure 5 shows the rate coefficient, k_{obs}, for H_2O_2 decomposition in the presence of 0.5 g of Al_2O_3 at 100 °C as a function of

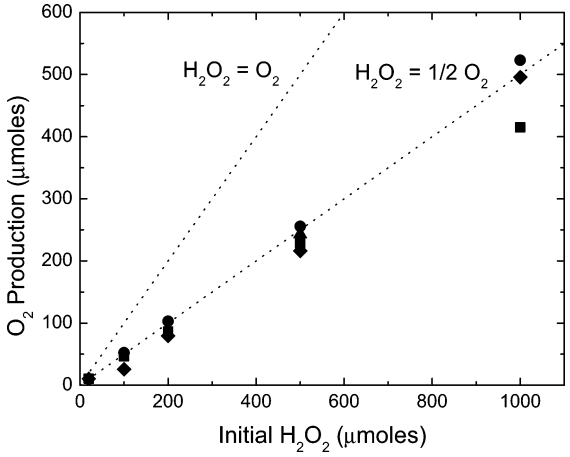

Figure 6. Production of O_2 as a function of initial H_2O_2 concentration at 25 °C for SiO_2 (●), Al_2O_3 (■), TiO_2 (▲), and ZrO_2 (◆). The dashed lines show the expected amount of O_2 for different stoichiometries.

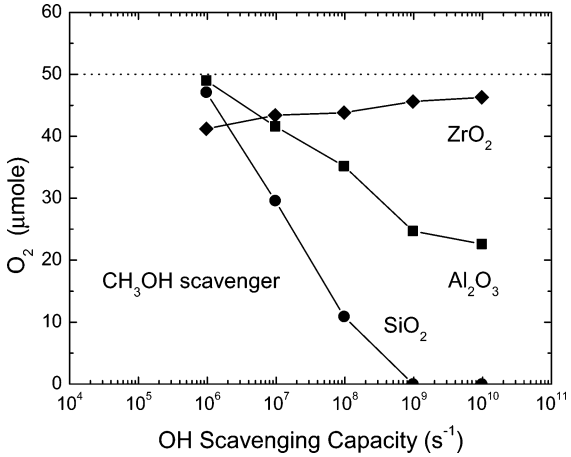

Figure 7. Production of O_2 as a function of OH scavenging capacity of methanol at 25 °C for SiO_2 (●), Al_2O_3 (■), and ZrO_2 (◆). The dashed lines show the expected amount of O_2 for complete decomposition of 2 mL of 50 mM H_2O_2 to $^1/_2O_2$.

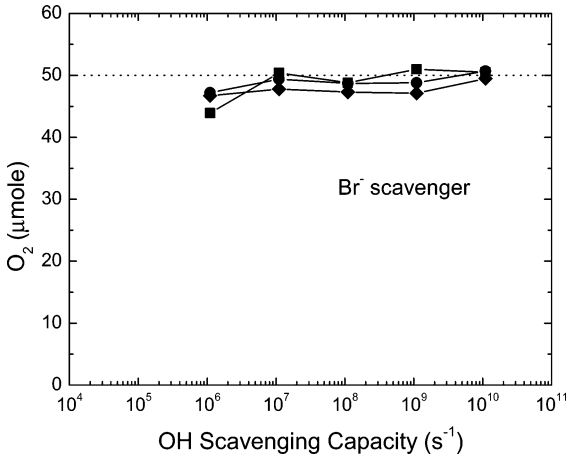

Figure 8. Production of O_2 as a function of the OH scavenging capacity of bromide at 25 °C for SiO_2 (●), Al_2O_3 (■), and ZrO_2 (◆). The dashed lines show the expected amount of O_2 for complete decomposition of 2 mL of 50 mM H_2O_2 to $^1/_2O_2$.

initial H_2O_2 concentration. The rate coefficient seems invariant below about 50 μM but decreases with increasing initial concentration of H_2O_2. Moreover, from Arrhenius plots for H_2O_2 decomposition with various initial concentrations, it is found that the activation energy increases with an increase of the initial concentration. The activation energy for H_2O_2 decomposition in the presence of 0.5 g of Al_2O_3 increases to 67 kJ/mol at a concentration of 50 mM H_2O_2. This value for the activation energy is very close to the 71 kJ/mol found by Takagi and Ishigure at an H_2O_2 concentration of about 7 mM.[9] Such changes in the rate coefficient and the activation energy indicate an increased stability of H_2O_2 as the initial concentration increases. All of the measurements of H_2O_2 decay showed first-order kinetics with depletion down to about 5% of initial H_2O_2. Yet the data in Figure 5 show that the rate coefficient for decay is dependent on the initial H_2O_2 concentration. This observation could be due to the saturation of active sites on the oxide surface available for adsorption of H_2O_2. Equilibrium between adsorption and desorption should exist, but it may be on a rate slower than that of the experiments so an overall first-order decay is observed. Further experiments will be performed by increasing the available surface sites, i.e., increased fraction of oxide, and examining the effects due to other oxides.

Gaseous Products in the Decay of H_2O_2. An attempt was made to acquire more information on the mechanism of H_2O_2 decay by examining product formation. From reactions R1 and R1a, the obvious gaseous product to monitor is molecular oxygen. Samples of 11 wt % oxides, 0.25 g per 2 mL of aqueous solution, were prepared, outgassed, and left at 25 °C for 10 half-lives as determined from the data of Table 1. This time was sufficient for H_2O_2 to decay beyond all trace, which was confirmed by H_2O_2 analysis. The production of O_2 is shown in Figure 6 as a function of initial H_2O_2 concentration for SiO_2, Al_2O_3, TiO_2, and ZrO_2. In all cases, the stoichiometry is $H_2O_2 = {}^1/_2O_2$ as given by R4 and predicted by reactions R1−R3.

The results of the previous sections show that decomposition of H_2O_2 is dependent on the presence of oxide interfaces, and at least part of the chemistry is expected to occur on the surface. Several studies have suggested that OH or HO_2 radicals may exist in the bulk water.[14,16−19,26,28] Scavenging of these radicals should have an effect on O_2 formation. Several scavenger studies were performed under similar conditions as in the previous section on gas production, except with the addition of varying concentrations of radical scavengers. Figure 7 shows the formation of O_2 for aqueous solutions of 50 mM H_2O_2 and 0.25 g of SiO_2, Al_2O_3, or ZrO_2 with different initial concentrations of methanol. Gas production is shown as a function of the scavenging capacity of the solution for OH radicals, where the scavenging capacity is given by the product of the methanol concentration and the scavenging rate coefficient ($k = 9.7 \times 10^8\ M^{-1}s^{-1}$).[50] Complete decay of H_2O_2 in these systems should give 50 μmol of O_2 as indicated by the dashed line in Figure 7. Increasing methanol concentration decreases the production of H_2O_2 with SiO_2 and to a lesser extent with Al_2O_3, but it has very little effect with ZrO_2. If reactions R1−R3 are valid for describing the mechanism, then it would appear that in some cases methanol can compete with H_2O_2 in reaction R2 for OH radicals.

Bromide is also an efficient OH radical scavenger ($k = 1.1 \times 10^{10}\ M^{-1}s^{-1}$)[50] and can be used to probe for the presence of this radical in the bulk water. Figure 8 shows the production of O_2 as a function of the scavenging capacity of Br^- for OH radicals in aqueous solutions of 50 mM H_2O_2 and 0.25 g of SiO_2, Al_2O_3, or ZrO_2. Bromide does not seem to have any noticeable effect on O_2 formation even though it is a much better scavenger of OH radicals than methanol. It is not likely that the adduct, $BrOH^-$, or its daughters could be decaying to O_2. The obvious conclusion is that OH radicals do not escape into the bulk water. If reactions R1 and R2 occur, then they must be on the surface of the oxide. However, methanol can adsorb

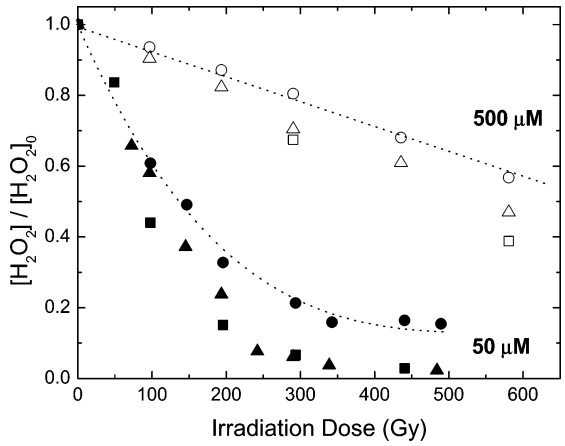

Figure 9. Radiolytic decomposition of H_2O_2 as a function of dose for 50 μM H_2O_2 and no added oxide (●), 0.5 g Al_2O_3 (▲), and 1.0 g Al_2O_3 (■); 500 μM H_2O_2 and no added oxide (○), 0.5 g Al_2O_3 (△), and 1.0 g Al_2O_3 (□).

on the surface of the oxides examined here.[51,52] Sufficient adsorbed methanol could interfere with reactions R1 and R2 occurring on the surface, as observed with SiO_2 and Al_2O_3. At the highest methanol concentrations, small amounts (~5 μmol) of H_2 are also observed in the SiO_2 and Al_2O_3 suspensions, not shown. Hydrogen is not observed in any other system examined here and suggests that methanol decomposition is occurring in the process of O_2 suppression. Further studies varying the pH may be used to adjust the adsorption fraction of scavengers and thereby examine surface scavenging of radicals in more detail.

H_2O_2 Decomposition in the γ-Radiolysis of Water with Oxides. The γ-radiolysis of aqueous H_2O_2 solutions has been examined under a variety of conditions.[37−42] As expected, the radicals produced in the decomposition of water led to decomposition of the H_2O_2. However, the effects of added oxides on H_2O_2 decomposition in the γ-radiolysis of water have not been previously examined. Figure 9 shows the depletion of H_2O_2 in the γ-radiolysis of water in the presence and absence of oxides. Deaerated solutions of 50 μM and 500 μM initial concentrations were examined. The decay of H_2O_2 occurs by many different pathways, but the main component is due to its reaction with the hydrated electron ($k = 1.1 \times 10^{10}$ M^{-1} s^{-1}).[50]At high doses, the H_2O_2 concentration will plateau when its production equals its decomposition.[41] It can be seen that a dose of about 400 Gy is sufficient for 50 μM H_2O_2 to reach a constant value at 20% of its initial concentration. Much higher doses are required for 500 μM H_2O_2 solutions, simply because more radicals are required to reach equilibrium. The addition of 0.5 or 1.0 g of Al_2O_3 also shows a decrease in H_2O_2 concentration with increasing dose. Similar results were observed with SiO_2 suspensions. With a sufficient dose, the H_2O_2 concentration decreases to essentially zero with 50 μM H_2O_2 solutions, and similar results will probably be observed with 500 μM H_2O_2 solutions at higher doses. The presence of Al_2O_3 increases the decomposition of H_2O_2, and a small effect on Al_2O_3 surface area is observed. Uncertainties in the measurements and the complexity of the reactions may mask the magnitude of the surface area effect. One possible reason for any surface area effect is due to the production of additional hydrated electrons by energy deposition in the oxides. In this scenario, energy deposited by the radiation oxide is able to pass to or through the particle surface into the bulk water. A similar effect was observed for H_2 production in the radiolysis of aqueous SiO_2 mixtures.[43] Of course, electrons or other energy carriers may just reach the surface of the particle and decompose any adsorbed H_2O_2. Further studies with different oxides of various dimensions and with added radical scavengers will lead to more information on energy transfer from the particle to bulk water and hopefully indicate whether surface or bulk water reactions are involved.

Conclusions on the Mechanism of H_2O_2 Decomposition in Aqueous Oxide Mixtures

While the evidence presented here is not sufficient to definitively determine the mechanism for H_2O_2 decomposition in the presence of water−oxide interfaces, certain aspects of the reaction involved are elucidated. The decomposition of H_2O_2 in liquid water traditionally has been described using reactions R1−R3 and R5. Stoichiometric O_2 production seems to confirm $H_2O_2 = {}^1/_2O_2$ in agreement with these reactions. The rate of H_2O_2 decomposition increases with the addition of some ceramic oxides. In some cases, such as with CeO_2 and ZrO_2, the increase in H_2O_2 decomposition rate is dramatic, showing the strong influence of the oxide interface. Studies seem to show that the increase in H_2O_2 decomposition is linear with available surface area but not only dependent on surface area. That is; even at equivalent surface areas, the various oxides have different rates for H_2O_2 decomposition. These variations in decay rates may be due to differences in number of reactive sites or in their efficiency. Scavenger studies suggest that H_2O_2 decomposition occurs on the surface with OH or HO_2 radical escape to the bulk observed for only some ceramic oxides. On some ceramic oxides, much, if not all, of the H_2O_2 decomposition occurs on the surface. The radiolytically induced destruction of H_2O_2 in aqueous solutions increases with the addition of oxide particles. This increase is thought to be due to the energy transfer from the solid oxide to or through the oxide−water interface. The exact precursor to H_2O_2 decomposition is not known, nor if the reaction is at the surface or in the bulk water.

Acknowledgment. The research described herein was supported by the Office of Basic Energy Sciences of the U.S. Department of Energy. This contribution is NDRL-4543 from the Notre Dame Radiation Laboratory.

References and Notes

(1) Croiset, E.; Rice, S. F.; Hanush, R. G. *AIChE J.* **1997**, *43*, 2343.
(2) Bessa, E.; Sant'Anna, G. L., Jr.; Dezotti, M. *Appl. Catal., B.* **2001**, *29*, 125.
(3) Cowan, R. L. *Nucl. Energy (Br. Nucl. Energy Soc.)* **1997**, *36*, 257.
(4) Haber, F.; Weiss, J. *Proc. R. Soc. London, Ser. A* **1934**, *147*, 332.
(5) Giguere, P. A.; Liu, I. D. *Can. J. Chem.* **1957**, *35*, 283.
(6) Kijewski, H.; Troe, J. *Int. J. Chem. Kinet.* **1971**, *3*, 223.
(7) Tessier, A.; Forst, W. *Can. J. Chem.* **1974**, *52*, 794.
(8) Baulch, D. L.; Cobos, C. J.; Cox, R. A.; Frank, P.; Hayman, G.; Just, Th.; Kerr, J. A.; Murrells, T.; Pilling, M. J.; Troe, J.; Walker, R. W.; Warnatz, J. *J. Phys. Chem. Ref. Data* **1994**, *23*, 847.
(9) Gray, P. *Trans. Faraday Soc*. **1959**, *55*, 408.
(10) Takagi, J.; Ishigure, K. *Nucl. Sci. Eng.* **1985**, *89*, 177.
(11) Hart, A. B.; McFadyen, J.; Ross, R. A. *Trans. Faraday Soc*. **1963**, *59*, 1458.
(12) Hoare, D. E.; Peacock, G. B.; Ruxton, G. R. D. *Trans. Faraday Soc*. **1967**, *63*, 2498.
(13) Roy, C. B. *J. Catal*. **1968**, *12*, 129.
(14) Kitajima, N.; Fukuzumi, S.; Ono, Y. *J. Phys. Chem.* **1978**, *82*, 1505.
(15) Klissurski, D.; Hadjiivanov, K.; Kantcheva, M.; Gyurova, L. *J. Chem. Soc., Faraday Trans.* **1990**, *86*, 385.
(16) Ono, Y.; Matsumura, T.; Kitajima, N.; Fukuzumi, S. *J. Phys. Chem.* **1977**, *81*, 1307.
(17) Arutyunyan, A. Zh.; Grigoryan, G. L.; Nalbandyan, A. B. *Kinet. Catal.* **1985**, *26*, 785.
(18) Arutyunyan, A. Zh.; Grigoryan, G. L.; Nalbandyan, A. B. *Kinet. Catal.* **1986**, *27*, 1352.
(19) Arutyunyan, A. Zh.; Gazaryan, K. G.; Garibyan, T. A.; Grigoryan, G. L.; Nalbandyan, A. B. *Kinet. Catal*. **1988**, *29*, 880.

(20) Amorelli, A.; Evans, J. C.; Rowlands, C. C. *J. Chem. Soc., Faraday Trans. 1*, **1988**, *84*, 1723.
(21) Giamello, E.; Fubini, B.; Voltante, M.; Costa, D. *Colloids Surf.* **1990**, *45*, 155.
(22) Giamello, E.; Volante, M.; Fubini, B.; Geobaldo, F.; Morterra, C. *Mater. Chem. Phys.* **1991**, *29*, 379.
(23) Giamello, E.; Calosso, L.; Fubini, B.; Geobaldo, F. *J. Phys. Chem.* **1993**, *97*, 5735.
(24) Giamello, E.; Rumori, P.; Geobaldo, F.; Fubini, B.; Paganini, M. C. *Appl. Magn. Reson.* **1996**, *10*, 173.
(25) Murphy, D. M.; Griffiths, E. W.; Rowlands, C. C.; Hancock, F. E.; Giamello, E. *Chem. Commun.* **1997**, 2177.
(26) Lin, S. S.; Gurol, M. D. *Environ. Sci. Technol.* **1998**, *32*, 1417.
(27) Anpo, M.; Che, M.; Fubini, B.; Garrone, E.; Giamello, E.; Paganini, M. C. *Top. Catal.* **1999**, *8*, 189.
(28) Miller, C. M.; Valentine, R. L. *Water Res.* **1999**, *33*, 2805.
(29) Hochanadel, C. J. *Radiat. Res.* **1962**, *17*, 286.
(30) Einschlag, F. G.; Feliz, M. R.; Capparelli, A. L. *J. Photochem. Photobiol., A* **1997**, *110*, 235.
(31) Emilio, C. A.; Jardim, W. F.; Litter, M. I.; Mansilla, H. D. *J. Photochem. Photobiol., A* **2002**, *151*, 121.
(32) Cater, S. R.; Stefan, M. I.; Bolton, J. R.; Amiri, A. S. *Environ. Sci. Technol.* **2000**, *34*, 659.
(33) Yeh, C. K. J.; Kao, Y. A.; Cheng, C. P. *Chemosphere* **2002**, *46*, 67.
(34) Kwan, W. P.; Voelker, B. M. *Environ. Sci. Technol.* **2002**, *36*, 1467.
(35) He, J.; Ma, W.; He, J.; Zhao, J.; Yu, J. C. *Appl. Catal., B* **2002**, *39*, 211.
(36) Ravikumar, J. X.; Gurol, M. D. *Environ. Sci. Technol.* **1994**, *28*, 394.
(37) Fricke, H. *J. Chem. Phys.* **1934**, *3*, 364.
(38) Hart, E. J.; Matheson, M. S. *Discuss. Faraday Soc.* **1952**, *12*, 169.
(39) Anderson, A. R.; Hart, E. J. *J. Phys. Chem.* **1961**, *65*, 804.
(40) Buxton, G.; Wilmarth, W. K. *J. Phys. Chem.* **1967**, 2835.
(41) Pastina, B.; LaVerne, J. A. *J. Phys. Chem. A* **2001**, *105*, 9316.
(42) Stefanic, I.; LaVerne, J. A. *J. Phys. Chem. A* **2002**, *106*, 447.
(43) LaVerne, J. A.; Tonnies, S. E. *J. Phys. Chem. B* **2003**, *107*, 7277.
(44) Ishigure, K. In *Water Chemistry of Nuclear Reactor Systems 5*; British Nuclear Energy Society: London, 1989; p 91.
(45) Haines, R. I.; McCracken, D. R.; Rasewych, J. B. In *Water Chemistry of Nuclear Reactor Systems 5*; British Nuclear Energy Society: London, 1989; p 309.
(46) McCracken, D. R.; Tsang, K. T.; Laughton, P. J. *Aspects of the Physics and Chemistry of Water Radiolysis by Fast Neutrons and Fast Electrons in Nuclear Reactors*; AECL 11895; Atomic Energy of Canada Limited: Chalk River, CA 1998.
(47) Schuler, R. H.; Allen, A. O. *J. Phys. Chem.* **1956**, *24*, 56.
(48) Hochanadel, C. J. *J. Phys. Chem.* **1952**, *56*, 587.
(49) Ghormley, J. A.; Stewart, A. C. *J. Am. Chem. Soc.* **1956**, *78*, 2934.
(50) Buxton, G. V.; Greenstock, C. L.; Helman, W. P.; Ross, A. B. *J. Phys. Chem. Ref. Data* **1988**, *17*, 513.
(51) Binet, C.; Daturi, M. *Catal. Today* **2001**, *70*, 155.
(52) Novak, E.; Hancz, A.; Erdohelyi, A. *Radiat. Phys. Chem.* **2003**, *66*, 27.